crystals

MDPI

Article

Photonic Bandgap–Cholesteric Device with Electrical Tunability and Optical Tristability in Its Defect Modes

Po-Chang Wu [1], Chih-Yuan Hsiao [2] and Wei Lee [1,*]

[1] Institute of Imaging and Biomedical Photonics, College of Photonics, National Chiao Tung University, Guiren District, Tainan 71150, Taiwan; jackywu0327@yahoo.com.tw

[2] Institute of Photonic System, College of Photonics, National Chiao Tung University, Guiren District, Tainan 71150, Taiwan; kjoe800818@gmail.com

* Correspondence: wlee@nctu.edu.tw; Tel.: +886-6-303-2121 (ext. 57826); Fax: +886-6-303-2535

Academic Editor: Charles Rosenblatt

Received: 14 May 2017; Accepted: 20 June 2017; Published: 23 June 2017

Abstract: This study proposes a hybrid structure for a one-dimensional (1D) photonic crystal (PC) comprising a tristable cholesteric liquid crystal (CLC) as the defect layer. The CLC exhibits three optically stable states: the Grandjean planar (P), focal conic (FC), and uniform lying helix (ULH) configurations. Specifically, the reflection band of the CLC is set within the photonic bandgap (PBG) of the 1D PC. While the ULH and the FC states can be regarded as the light-on and light-off states for defect-mode peaks in the visible spectrum, respectively, switching the device from the ULH to the P state enables suppression of the transmission of partial defect modes within the PBG. This device possesses many alluring features, such as optical tristability at null applied voltage and transmission tunability of the defect modes, providing a new pathway for the design of multifunctional and energy-efficient optical switches, light shutters, multichannels, and wavelength selectors.

Keywords: photonic crystals; cholesteric liquid crystals; energy-efficient photonic devices

1. Introduction

Photonic crystals (PCs) have long been an intriguing research area in optics, since two pioneering works by Yablonovich [1] and John [2] were independently published in the late 1980's. Typically, PCs are natural or artificial substances with spatial periodicity of dielectric constant, as well as a refractive index in a certain dimension, giving rise to the formation of a specific region known as the photonic bandgap (PBG) in their spectral properties. Analogously to the concept of the electronic bandgap in semiconductors for electrons, the PBG of PCs is responsible for forbidding the propagation of some photons whose wavelengths lie within its bandgap. When a defect layer is inserted in a PC, defect-mode peaks in the spectrum, enabling the transmission of photons, will be generated within the PBG as a result of breaking the structural periodicity. Based on such a hybrid design, numerous studies concerning the use of liquid crystal (LC) as the defect layer, sandwiched between a pair of dielectric multilayers—i.e., by a one-dimensional (1D) PC—have been extensively reported since 2002 [3]. The attraction of a 1D PC/LC stems from the tunable optical nature of defect modes, attributable to the stimuli-responsive material properties of LCs. For instance, the tunability in defect-mode wavelength has been achieved in 1D PC hybrids, with a planar-aligned nematic and a twisted–nematic LC defect layer via the electrically/magnetically controlled birefringence and the adiabatic following effects, respectively [3–5]. In addition, utilizing individual LC modes featuring dynamic scattering as a defect layer, such as polymer-dispersed nematic LC [6], smectic-A LC [7] and cholesteric LC (CLC) [8,9], continuous and reversible variation in transmission of defect modes

has also been demonstrated based on the voltage-induced reorientation of LC molecules (from a light-scattering state to a light-transparent state, and vice versa) manipulated by voltage or light. Moreover, the spectral properties of symmetric and asymmetric 1D PC with CLC [10,11], bistable chiral–splay nematic (BCSN) [12], or planar-aligned LC modes [13] have been investigated, and these hybrid structures proposed for applications in tunable lasers.

From the point of view of environmental protection, there is a great desire for photonic devices with low power consumption in order to meet the demand for green concepts, including energy saving and carbon reduction. Consequently, apart from the aforementioned hybrid 1D PC devices operating in the LC dynamic mode, Wu et al. established the first energy-efficient 1D PC/LC structure in 2011 by introducing a bistable chiral–homeotropic nematic (BHN) as the defect layer [14]. Later, the electrical switchability and optical multistablity of defect-mode peaks in the stable states of various photonic bandgap structures with bi- or tri-stable LCs, such as smectic-A LC [7], CLCs [8,9] and BCSN [15], have progressively been clarified in accordance with their driving schemes for textural switching.

CLCs are known for their helical molecular structure, periodically self-assembling in one dimension; thus, they can be regarded as a class of soft 1D PC, with a reflection band characterized by the average refractive index of the LC material, and the helical pitch induced by the chirality [16]. According to the orientation of molecular helical order direction (i.e., the helical axis), cholesteric textures—including the Grandjean planar (P), the focal conic (FC) and the fingerprint states—with distinct optical features have been well documented in the literature. Typically, both the P and FC textures are optically stable states in a planar-aligned CLC cell, and they are reversibly switchable by the electric field [17]. The P state with helical axes perpendicular to the substrate plane reflects circularly polarized light with the same handedness, whereas the FC state with randomly oriented helices scatters unpolarized light. On the other hand, the uniform lying helix (ULH) texture obtained in short-pitch CLCs constitutes a class of the fingerprint texture. The ULH texture exhibits unidirectional helical axes aligned in parallel to the substrate plane, and behaves as a uniaxial optical plate cut along the optic axis, where the helical axis takes the role of the optic axis of the plate. This texture does not scatter or reflect the incoming light, so its optical transparency is similar to that of the field-induced helix-free homeotropic (H) state of the cholesteric cell [18]. Unlike the P and the FC states which can stably be obtained by surface aligning treatment, the ULH texture has long been proven difficult in terms of creating monodomain alignment with high stability in a simple sandwich cell geometry.

Recently, an approach allowing the ULH texture to be stably obtained in a planar-aligned CLC has been reported by means of a low-frequency voltage pulse to induce the electrohydrodynamic (EHD) effect [19]. A tristable CLC with P, FC and ULH textures as steadfast states is thus proposed. The ULH state, typically realized in short-pitch CLCs, is a class of the fingerprint texture. The optical transparency of the ULH is comparable to that of the homeotropic (H) state in that it can be regarded as a uniaxial crystal. To date, possible applications of this tristable CLC have been suggested for the switchable reflector in a transflective display [20], and the optical switch for the control of the polarization of fluorescent light [21]. In this study, we focus on the driving scheme for textural switching among the stable P, FC and the ULH states, and present a tristable 1D PC/CLC device based on their spectral features. Compared with other hybrid structures containing CLC as the defect layer, the Bragg reflection band of the CLC considered in this work is designed to be within the PBG of the 1D PC. The transmission of certain defect modes within the overlapped wavelength region is hence expectedly and considerably suppressed. Moreover, two stable FC states, designated FC-1 and FC-2, differing in domain sizes, are distinguished by modulating the frequency of the applied voltage. The spectral properties of the 1D PC/CLC cell in various cholesteric textures are discussed for the single-polarizer scheme where a linear polarizer is inserted between the light source and the cell. Potential applications of the proposed PBG structure are suggested, based on the electrical tunability and optical tristability of the spectral peaks of defect modes.

2. Experiment

The hybrid PC structure was fabricated by sandwiching an 8-μm-thick CLC bulk between two dielectric multilayers, as illustrated in Figure 1a. The two dielectric mirrors (i.e., multilayers on transparent substrates) are identical, each comprising five layers of high-refractive-index material (Ta_2O_5; with refractive index n_H = 2.18 and layer thickness d_H = 68.09 nm), and four layers of low-refractive-index material (SiO_2; n_L = 1.47 and d_L = 102.37 nm), which were deposited alternately on an indium–tin-oxide (ITO)-coated glass substrate. The multilayer exhibits a PBG with a central wavelength of ~600 nm and width of 290 nm, ranging from 470 to 740 nm [14]. Let's ignore the fraction of incident energy that is absorbed at each reflection. According to the transmission spectrum of a single dielectric mirror, as shown in Figure 1b, the transmittance T at the central wavelength (i.e., 600 nm) of the PBG is ~0.084. The reflectance R of the dielectric mirror, as determined by the simple relation of $T + R = 1$, is thus approximately equal to 0.916. Each dielectric mirror was spin-coated with a polyimide film (SE-150, Nissan Chem., Tokyo, Japan), followed by mechanical rubbings in anti-parallel directions to induce planar alignment of LC molecules for the assembled cell. On the other hand, the CLC was made of a nematic host E7 (Daily-Polymer Co., Kaohsiung, Taiwan) doped with 2.34-wt% right-handed chiral agent R5011 (HCCH, China). The helical twisting power of R5011 in E7 is 107 μm^{-1} and the refractive indices of E7 are n_e = 1.747 and n_o = 1.522 at the wavelength of 589.3 nm and temperature of 20 °C. Figure 1b displays the transmission spectra of an empty PC cell consisting of two multilayers separated by an air gap and of a regular planar-aligned CLC cell without multilayered coatings on the substrates. The empty cell reasonably yields "intense" defect-mode peaks within the PBG of the PC cell, since the refractive index of the air is inconsistent with those of the two dielectric materials. For normal incidence, the values of the linear free spectral range $\Delta\lambda$, defined as the separation between adjacent orders of interference (i.e., two neighboring intense defect-mode peaks), are greater than 20 nm, ranging from 21 nm to 29 nm for the defect modes within the PBG. For example, the 597-nm peak (with a full width at half maximum $\delta\lambda$ = 1.73 nm) exhibits $\Delta\lambda \approx 27$ nm. In addition, the reflecting finesse F defined as $\pi R^{1/2}(1 - R)^{-1}$ is calculated to be *ca* 36. On the other hand, the spectrum of the CLC exhibits a reflection band with the central wavelength of ~610 nm and bandwidth of ~88 nm ranging from 565 nm to 653 nm.

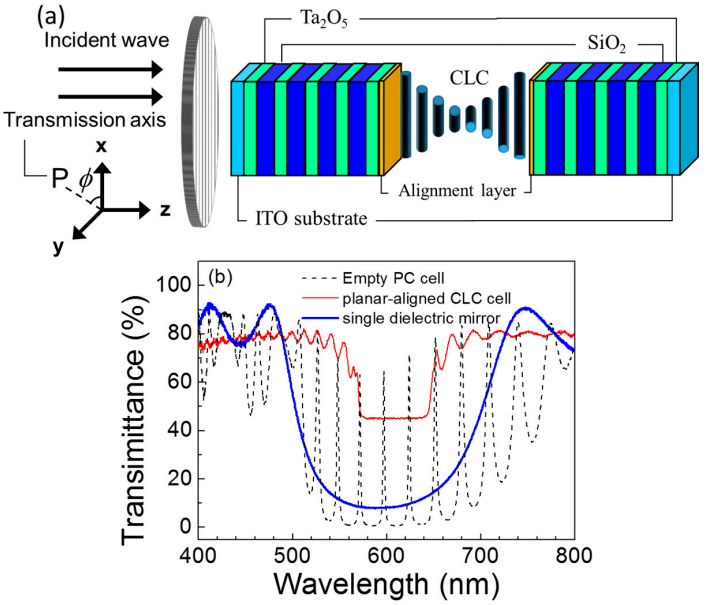

Figure 1. (**a**) Schematic of the 1D PC/CLC cell and (**b**) transmission spectra of the single dielectric mirror, empty PC cell with an air gap of 8 μm and a planar-aligned CLC cell without multilayer coatings on the substrates.

Accordingly, when injecting the CLC into the empty PC, one can see from Figure 1b that the Bragg reflection band of the CLC is located within the PBG of the 1D PC, accomplishing the intended structural design of the PC/CLC cell in the present study. All measurements were performed at room temperature. It has previously been demonstrated that the reflection band of the CLC mixture (E7 + R5011) exhibits only a small variation (~5 nm) in the temperature range between 18 °C and 54 °C [22,23]. Therefore, the effect of change in ambient temperature on the spectral properties of the 1D PC/CLC cell can be properly precluded.

The switching among the CLC textures in the PC/CLC cell was carried out by various square-wave voltage pulses, supplied with an arbitrary function generator (Tektronix AFG-3022B) together with a power amplifier (TREK Model 603). A polarizing optical microscope (Olympus BX51) was employed to confirm each CLC texture. The spectral profiles of the sample in the visible regime were acquired with a high-speed fiber-optic spectrometer (Ocean Optics HR2000+) in conjunction with a halogen light source (Ocean Optics HL2000). Meanwhile, a linear polarizer was situated between the light source and the cell. As shown in Figure 1a, the cell is set in the *x*-*y* plane with rubbing directions parallel to the *x* axis and unpolarized white light propagated along the *z* axis. The polarization angle between the rubbing direction of the front substrate (i.e., the ULH helical axis) and the transmission axis of the polarizer is defined as ϕ ($0^\circ \leq \phi \leq 90^\circ$) varying in the *x*-*y* plane; thus, the unpolarized incident light can be distinguished for the ordinary and extraordinary components by setting the polarization angle at $\phi = 0^\circ$ and $\phi = 90^\circ$, respectively.

3. Results and Discussion

3.1. Textural Formations in the CLC Defect Layer and the Driving Scheme

This part is aimed at clarifying the operation of the CLC defect layer, including the critical conditions for the voltage-induced CLC textures and their switching, the stability of stable CLC states, and the switching time between two arbitrary CLC textures. Figure 2 illustrates the driving scheme for various switching routes among all possible CLC states in the 1D PC/CLC cell. Here, the solid and dashed arrows indicate switching from one to another texture with increasing and descending amplitude or frequency of an applied voltage, respectively. Upon the application of increasing voltage pulses V at frequency f_1 = 30 Hz, the CLC texture in the initial P state changes sequentially to the FC-1, ULH, FC-2, and the H states. The corresponding optical images shown in Figure 2 were taken at V = 0 V for the P state, $V_{\text{FC-1}}$ = 15 V for the FC-1 state, V_{ULH} = 22 V for the ULH state, $V_{\text{FC-2}}$ = 35 V for the FC-2 state, and V_{H} = 50 V for the H state. It is worth mentioning that, except for the H state, the other four states (namely, P, FC-1, ULH, FC-2) can be preserved with distinct degrees of stability after the removal of designated voltages. The P, FC, and ULH textures have previously been claimed to be stable states in CLCs with central wavelengths in the visible range, and their long-term stability has been well verified while considering the tristable CLC for proper applications [16–18]. In the designated PC/CLC structure, both the P and FC textures revealed excellent stability, showing lifetimes of at least a week. In contrast, the stability of the ULH texture was comparably low, and could only be stably obtained for a limited period of time (approximately 6 h), tending to relax to the P state over time. The relatively lower stability in the ULH state could be a result of the low energy barrier between it and the P state, attributable to the imperfect cell conditions and alignment uniformity. As suggested previously, one could consider promoting the stability of the ULH state by shortening the helical pitch and reducing the cell gap [19], or by doping a proper amount of photocurable monomers to create polymer networks via the ultraviolet-light-induced photopolymerization [24]. Note that f_1 is low enough for the cell to induce the EHD effect. It has been clarified that the critical frequency regime for the induction of the EHD effect in a CLC cell is determined by dielectric relaxation behavior in the low-frequency regime, where the resulting complex dielectric spectra are dominated by the transport behavior of mobile ions within the cell [25]. Among all observed CLC textures, the ULH and the FC-2 states were created via the voltage-induced EHD effect. Here, EHD instability, determined

by the motion of ions, could be regarded as a crucial factor for realigning molecular helices with unidirectional helical axis, parallel to the rubbing direction, to form the ULH texture, along with randomly orientated helices to form the FC-2 state. The formation of the ULH state was attributable to the effective molecular flow, as well as the induction of horizontal shear stress within the bulk of the cell, whereas the FC-2 state resulted from the turbulence and the destabilization of CLC helices at a higher voltage. The ULH state was formed with its helical axis parallel to the rubbing direction; thus, it exhibited an almost dark appearance (with some defects generated), as the rubbing axis was parallel to the transmission axis of one of the crossed polarizers. Subsequently, while switching off the voltage, the helical configurations of the ULH and the FC-2 states in the voltage-off state were stably preserved, with neither molecular nor ionic perturbation. It is worth mentioning that the ULH and FC-2 textures, obtained via the EHD effect in this study, are in good agreement with previous studies, claiming them as stable states in planar-aligned CLCs with positive [19,25] or negative dielectric anisotropy [26,27]. In contrast, the FC-1 was generated by dielectric coupling between the LC molecules and the electric field, so that the value of $V_{\text{FC-1}}$ was lower than the onset voltage for triggering the EHD instability. It was confirmed from the textural appearances that the domain sizes in the FC-2 state were much smaller than those in the FC-1 state. They were thus identified in this driving scheme as two FC states with distinct domains. Figure 2 also indicates pathways for the direct switching between two certain states. Simply put, the ULH, FC-2 and H states can be directly switched from one to another by varying the voltage among V_{ULH}, $V_{\text{FC-2}}$ and V_{H} at a frequency of f_1. When increasing the frequency from f_1 = 30 Hz to f_2 = 1 kHz, backward switching from either the ULH or the FC-2 state to the FC-1 state can be achieved, due to the suppression in the ion-transport behavior, and thus the EHD flow within the bulk of the cell.

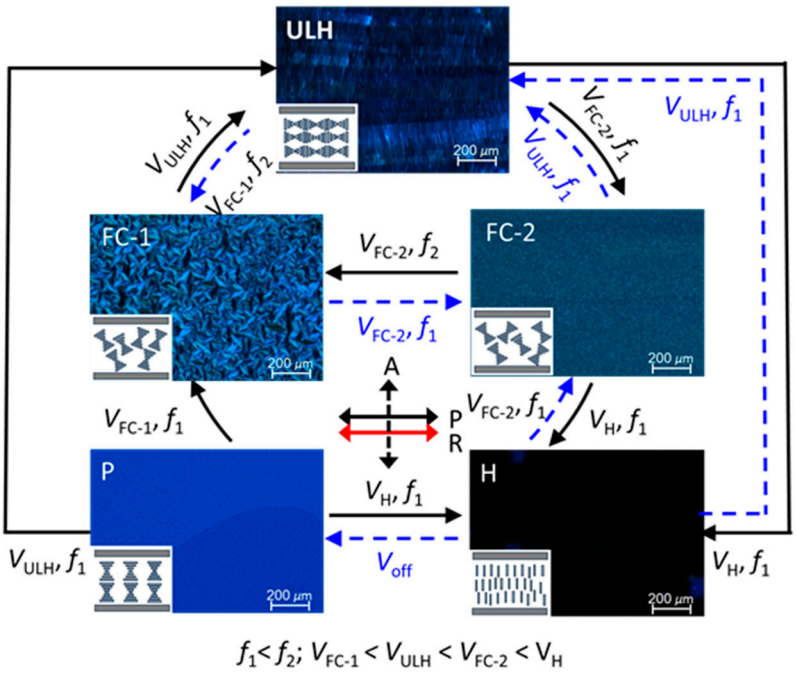

Figure 2. Schematic of the driving scheme for the voltage-induced switching among various CLC states and their corresponding optical textures in the 1D PC/CLC cell (scale bar: 200 μm). f_1 = 30 Hz, f_2 = 1 kHz; $V_{\text{FC-1}}$ = 15 V, V_{ULH} = 22 V, $V_{\text{FC-2}}$ = 35 V, V_{H} = 50 V.

The response time for the direct switching between two arbitrary CLC states by an external voltage was typically of the order of milliseconds at high frequencies (~kHz) due to the coupling between the LC molecules and the electric field, and of the order of seconds at low frequencies (e.g., 30 Hz), governed by the EHD effect. Based on the scheme for textural switching as shown in Figure 2, the

switching times from the P and ULH states to the FC-2 state by given voltages at f = 30 Hz were nearly 300 ms. In comparison, the response times from the P and FC-2 states to the ULH state were at least 4 s; the relatively slower speed for the formation of ULH state was presumably due to the time consumed for the realignment of molecular helices via the EHD effect. It should be remembered that the switching from the FC-1, ULH, or FC-2 state to the P state is indirect, implying a slow response, because it has to first switch to the H state and then to have the voltage promptly turned off. This disadvantage could be ruled out by means of a dual-frequency CLC [24].

3.2. Spectral Features of the 1D PC/CLC Cell in Various Cholesteric States

Based on the driving scheme as shown in Figure 2, the spectral properties of the 1D PC/CLC cell in various CLC states are further discussed in terms of the changes in refractive index and optical features of the CLC textures. Figure 3 shows the transmission spectra of the stable P, FC-1, ULH and FC-2 states at V = 0 and the voltage-sustained H state at V = 50 V of the 1D PC/CLC cell at the polarization angle $\phi = 90°$. The spectral features of the cell in the P, ULH and H states were dictated by the optical path length (OPL) and, thus, the effective refractive index of the CLC defect layer. The spectral profile becomes dependent on the light scattering strength in the FC-1 and the FC-2 states. In the case of $\phi = 90°$, the effective refractive index of the CLC is ideally equal to $(n_e + n_o)/2$ in the P and ULH states, and n_o in the H state. Owing to the shorter OPL in the H state as compared with those in the P and the ULH states, it can be seen from Figure 3 that the number of defect mode peaks with intense signal ranging between 470 nm and 740 nm (i.e., the width of the PBG of the 1D PC) in the H state (13) was smaller than those in the P (16) and ULH (14) states. The mismatch in the number of defect modes of the cell between the P and ULH states could be a result of non-uniform alignment in the ULH state, so that its effective refractive index would lie between $(n_e + n_o)/2$ and n_o. To inspect the abovementioned results, the transmission spectra of the cell in the P, H, and ULH states were simulated using the Jones 4 × 4 transfer matrix calculation. Here, we simply considered the three CLC states as isotropic mediums with distinct refractive indices, and the cell gap of the CLC layer was fixed to be 5.1 μm. By optimizing the refractive indices of the P, H, and ULH states to be n_P = 1.687, n_{ULH} = 1.613, and n_H = 1.522, respectively, the profile of each simulated transmission spectrum was nearly consistent with the experimental data. Consider the host LC E7 with known refractive indices of n_e = 1.747 and n_o = 1.522. It was found that the simulated refractive index of the CLC in the P state was higher than $(n_e + n_o)/2$, presumably due to the insufficient number of repeated helical pitches. Otherwise, the optimized refractive indices for the simulations in the H and ULH states were exactly equal to n_o and a value lying between $(n_e + n_o)/2$ and n_o, fully supporting our interpretations. In contrast, both the FC-1 and the FC-2 textures are scattering states, showing apparently weakened transmission in the same spectrum. On average, the transmittance in the FC-2 state was only around 1%, which was much lower than that of ~10% in the FC-1 state. For a CLC cell in the FC state, the scattering strength for incident light typically depends on the domain size, pitch length, and the birefringence of the LC. The superior ability for effective light-intensity suppression in the FC-2 state can thus be interpreted in terms of the formation of tiny domain sizes comparable to the wavelengths of incident light, and the effective mismatch of refractive indices between domains contributed by the randomness of molecular helices in the bulk of the cell. After evaluating the spectral features of the four abovementioned CLC textures, FC-1 was excluded for photonic applications in this work, because it shows a weaker light-scattering efficiency than that of FC-2. Namely, the three stable states, including P as the light-reflection state, ULH as the light-transparent state, FC-2 as the light-scattering state, are selected to manifest the tristable CLC.

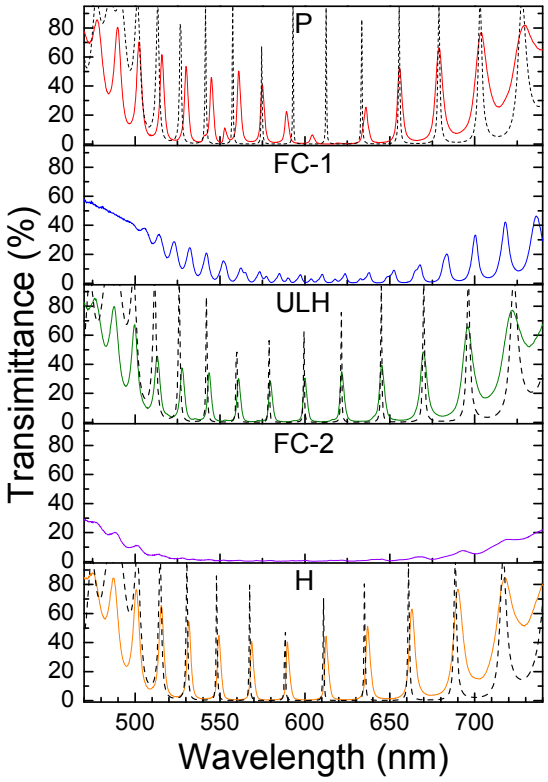

Figure 3. Transmission spectra of the five CLC states (P, FC-1, ULH, FC-2, and H) of the PC/CLC cell at $\phi = 90°$. The spectra, displayed with black dashed lines in the P, ULH, and H states, are the correspondingly simulated results.

3.3. Potential Applications of the 1D PC/CLC to Photonic Devices

Three potential applications of the proposed 1D PC/CLC cell as an energy-efficient photonic device are suggested in accordance with the spectral features of the three stable states and their tristable switching.

The first one is referred to as the textural switching between the P and the ULH state, enabling the design of the cell as a wavelength selector. In the P state, the spectrum exhibits pronounced defect-mode peaks within the PBG, except for those being suppressed in the reflection band (from 565 nm to 653 nm) of the CLC. This successfully reflects the idea of the suppression of defect modes in a certain wavelength range based on the proposed PBG structure. When switching the cell from the P to the ULH state, four noticeable defect-mode peaks appeared within the wavelength regime between 565 nm and 653 nm and the transmissions of the other defect modes well resembled those in the H state, suggesting stable and switchable defect modes in a designated wavelength region was achieved by P–ULH switching. Along this line, one could control the number of repressed defect modes prior to cell fabrication by optimizing the cell thickness and the refractive index of the nematic LC host to optimize the number of defect modes within the PBG of a hybrid PC cell and the bandwidth of the CLC. Moreover, a CLC characterized by a tunable reflection band could be introduced into the PC/CLC structure for the suppression of variable defect modes.

Secondly, while utilizing the ULH texture as the light-transparent state and the FC texture as the light-opaque state, the bistable switching between the ULH and the FC states made the cell applicable as a light shutter for multichannels across the entire PBG. It can be evaluated from Figure 3 that the contrast ratios of the light shutter were approximately 5 and 40 when employing FC-1 and FC-2, respectively, as the opaque state. Moreover, referring to the optical textures as shown in Figure 2, the spatial dependence of the transmission could be valid in the FC-1 state due to the non-uniform alignment and irregular domain sizes, whereas the FC-2 state with tiny domain sizes,

from a macroscopic viewpoint, showed an optically uniform domain distribution. This suggests constant light scattering strength over space when the cell is stabilized in the FC-2 state. Consequently, the PC/CLC cell as a light shutter could be created with high contrast and spatially independent optical properties based on switching between the ULH and FC-2 states.

Apart from the use of textural switching between two stable states, a third application of the 1D PC/CLC cell as a wavelength filter with two memorable sets of multichannels could be considered in the ULH state by varying the polarization angle.

Figure 4 depicts the spectral properties of the cell in the ULH state at three distinct polarization angles. The stable ULH state formed with the helical axis parallel to the rubbing direction behaves as a uniaxial crystal, so that the refractive index of the cell with a front polarizer is expected to be a function of the polarization angle. In the cases of $\phi = 0°$ and 90°, two sets of defect modes with different spectral profiles dedicated by the refractive indices of $n_{\parallel} = n_o$ and $n_{\perp} = (n_e + n_o)/2$ were realized, as shown in Figure 4a,c, respectively. At $\phi = 45°$, the spectrum became complex. As depicted in Figure 4b, double peaks in a defect mode actually belong to the ordinary and extraordinary components as they are decomposed at $\phi = 0°$ and 90°, respectively.

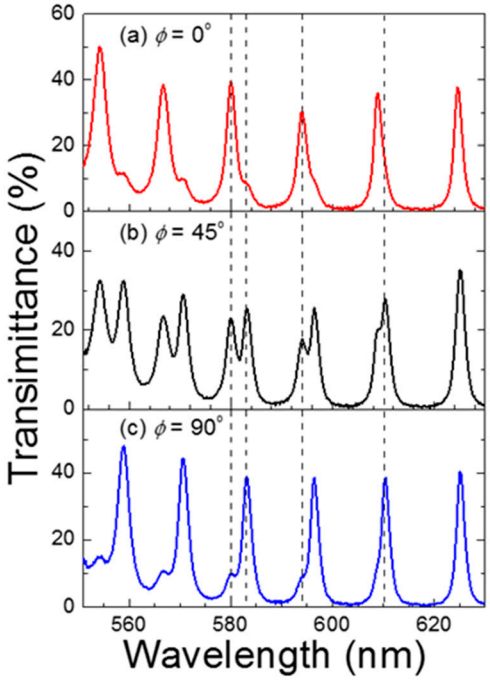

Figure 4. Transmission spectra of the PC/CLC cell in the ULH state at (**a**) $\phi = 0°$, (**b**) $\phi = 45°$ and (**c**) $\phi = 90°$. Here vertical dashed lines are plotted to highlight the peak positions of some defect modes in case (**b**).

Application of the proposed cell as an optical switch permits two stable and switchable sets of multichannels in the light-transmission ULH state (by simply adjusting the polarization angle to 0° and 90°). In comparison with the PC/CLC devices reported previously, the light-transmission state was the stable P texture in the bistable CLC [8], or the stable H texture in the tristable CLC [9]. Obviously, even when inserting a polarizer between the light source and the device, the defect modes would vary in neither case with the polarization angle, as the effective refractive index is constant, always $(n_e + n_o)/2$ in the P state and n_o in the H state. As such, only a set of defect modes could be allowed in previous designs.

In addition to the spectral profiles of the PC/CLC cell featuring optical stability in various CLC states, the application of the cell as an electrically tunable photonic device is also suggested based on the dynamically textural switching between the ULH and the FC-2 states. Figure 5 further demonstrates

the dynamic tunability of defect modes in the cell under the application of AC voltages at $\phi = 90°$. The cell was initially sustained in the ULH state at $V = 22$ V and $f = 30$ Hz. Figure 5a reveals that the transmittance of the defect modes gradually dropped with increasing voltage amplitude, reaching the minimum (<0.5%) in FC-2 at $V = 35$ V. In the meantime, a blue-shift of the defect modes of about 1.3 nm with increasing voltage amplitude from 22 V to 35 V was monitored, presumably due to the torque for helix unwinding at high voltages. Recall the driving scheme as shown in Figure 2. The mechanism of transmission tunability via voltage-controlled switching between the ULH as the transparent state, and the FC-2 state as the opaque state arises from the variation in EHD strength. Alternatively, the transport of mobile ions was restrained by increasing frequency at a fixed voltage of $V = 22$ V, leading to the reduction in EHD effect and, thus, the turbulence of molecules in the ULH state. As a result, the transmission of the defect modes, as shown in Figure 5b, increased with increasing frequency, maximizing and becoming saturated at $f = 1$ kHz due to the promotion in the uniformity of the ULH state. Similarly, slight blue-shift of defect-mode peaks by *ca.* 1.1 nm took place as the frequency increased from 30 Hz to 1 kHz.

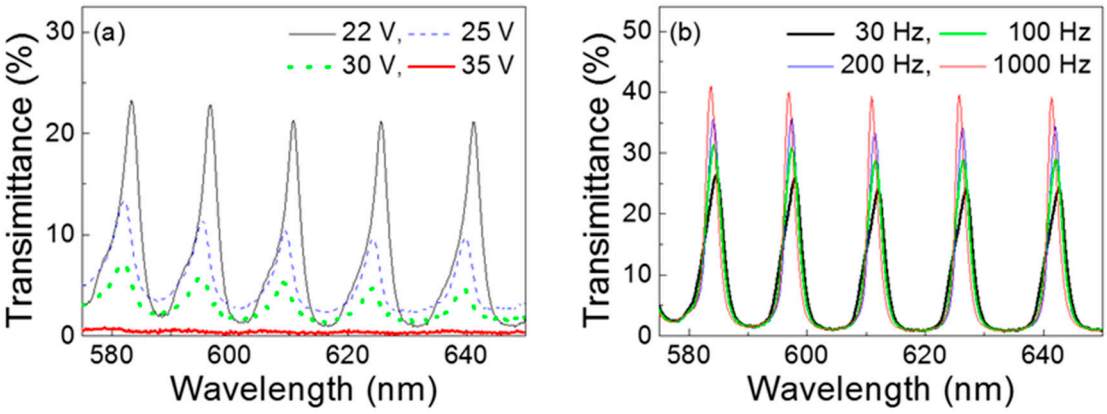

Figure 5. Transmission spectra of the PC/CLC cell at various (**a**) amplitudes ($f = 30$ Hz) and (**b**) frequencies ($V = 22$ V) of voltage pluses.

4. Conclusions

In summary, interesting characteristics of an electrically switchable and optically tristable multichannel device has been investigated. The proposed photonic structure was created by incorporating a CLC as a central defect layer in a 1D multilayer PC. One of the unique spectral features of this hybrid PC/CLC device is the reflection band of the CLC, which lies within the PBG of the 1D PC. Moreover, this hybrid structure possesses three stable states; *viz.*, the P, ULH and FC (including FC-1 and FC-2) states, thanks to the optical tristability of the CLC. According to the mechanism of the voltage-induced EHD effect, a driving scheme has been established, illustrating electrical switching among the stable states—P, ULH, FC-1 and FC-2—and the voltage-sustained H state. By inserting a linear polarizer between the light source and the cell, distinct spectral characteristics, such as partially and fully suppressed defect modes within the PBG in the P state, and high transmission of the defect modes in the ULH state, were obtained by electrical switching among the stable P, ULH and FC-2 states. This finding enables the applications of the PC/CLC cell as an energy-efficient multichannel filter for visible light communication, an optical switch and a wavelength selector. In particular, by varying the polarization angle, more than one set of stable defect-mode peaks with high transmission was realized in a sole PC/CLC cell, which outperforms previously reported PC/CLC devices in this regard. In addition to the optical tristability, the dynamically tunable defect modes were obtained by varying the frequency and amplitude of the applied AC voltage in order to control the ion transport and, in turn, the strength of the EHD effect. It was validated, based on the transmission spectra, that high contrast tuning in light transmission of defect modes is achievable by voltage-manipulated switching between

the ULH and the FC-2 states, making the 1D PC/CLC cell promising as an electrically controllable device for various photonic applications. It should be noted here that the fabrication process, involving the deposition of a dielectric multilayer on an ITO-coated substrate for the proposed 1D PC/CLC cell, can be rectified by technically coating the electrode layer on the top of the multilayer instead to prevent any energy waste from the structural design.

Acknowledgments: This work was financially supported by the Ministry of Science and Technology, Taiwan, under grant Nos. 104-2112-M-009-008-MY3 and 106-2923-M-009-002-MY3.

Author Contributions: Po-Chang Wu conceived and designed the experiments and drafted the manuscript. Chih-Yuan Hsiao performed the experiments and helped analyze the data. Wei Lee supervised the whole study and finalized the manuscript.

Conflicts of Interest: The authors declare no conflict of interest.

References

1. Yablonovitch, E. Inhibited Spontaneous Emission in Solid-State Physics and Electronics. *Phys. Rev. Lett.* **1987**, *58*, 2059–2062. [CrossRef] [PubMed]
2. John, S. Strong localization of photons in certain disordered dielectric superlattices. *Phys. Rev. Lett.* **1987**, *58*, 2486–2489. [CrossRef] [PubMed]
3. Ozaki, R.; Matsui, T.; Ozaki, M.; Yoshino, K. Electro-Tunable Defect Mode in One-Dimensional Periodic Structure Containing Nematic Liquid Crystal as a Defect Layer. *Jpn. J. Appl. Phys.* **2002**, *41*, L1482–L1484. [CrossRef]
4. Zyryanov, V.Y.; Myslivets, S.A.; Gunyakov, V.A.; Parshin, A.M.; Arkhipkin, V.G.; Shabanov, V.F.; Lee, W. Magnetic-field tunable defect modes in a photonic-crystal/liquid-crystal cell. *Opt. Express* **2010**, *18*, 1283–1288. [CrossRef] [PubMed]
5. Lin, Y.-T.; Chang, W.-Y.; Wu, C.-Y.; Zyryanov, V.Y.; Lee, W. Optical properties of one-dimensional photonic crystal with a twisted-nematic defect layer. *Opt. Express* **2010**, *18*, 26959–26964. [CrossRef] [PubMed]
6. Wu, P.-C.; Yeh, E.-R.; Zyryanov, V.Y.; Lee, W. Spatial and electrical switching of defect modes in a photonic bandgap device with a polymer-dispersed liquid crystal defect layer. *Opt. Express* **2014**, *22*, 20278–20283. [CrossRef] [PubMed]
7. Chen, C.-H.; Zyryanov, V.Y.; Lee, W. Switching of defect modes in a photonic structure with a tristable Smectic-A liquid crystal. *Appl. Phys. Express* **2012**, *5*, 082003. [CrossRef]
8. Hsiao, Y.-C.; Wu, C.-Y.; Chen, C.-H.; Zyryanov, V.Y.; Lee, W. Electro-optical device based on photonic structure with a dual-frequency cholesteric liquid crystal. *Opt. Lett.* **2011**, *36*, 2632–2634. [CrossRef] [PubMed]
9. Hsiao, Y.-C.; Hou, C.-T.; Zyryanov, V.Y.; Lee, W. Multichannel photonic devices based on tristable polymer-stabilized cholesteric textures. *Opt. Express* **2011**, *19*, 23952–23957. [CrossRef] [PubMed]
10. Matsuhisa, Y.; Ozaki, R.; Yoshino, K.; Ozaki, M. High Q defect mode and laser action in one-dimensional hybrid photonic crystal containing cholesteric liquid crystal. *Appl. Phys. Lett.* **2006**, *89*, 101109. [CrossRef]
11. Huang, J.-C.; Hsiao, Y.-C.; Lin, Y.-T.; Lee, C.-R.; Lee, W. Electrically switchable organo–inorganic hybrid for a white-light laser source. *Sci. Rep.* **2016**, *6*, 28363. [CrossRef] [PubMed]
12. Wang, H.-T.; Timofeev, I.V.; Chang, K.; Zyryanov, V.Y.; Lee, W. Tunable narrow-bandpass filter based on an asymmetric photonic bandgap structure with a dual-mode liquid crystal. *Opt. Express* **2014**, *22*, 15097–15103. [CrossRef] [PubMed]
13. Wang, H.-T.; Lin, J.-D.; Lee, C.-R.; Lee, W. Ultralow-threshold single-mode lasing based on a one-dimensional asymmetric photonic bandgap structure with liquid crystal as a defect layer. *Opt. Lett.* **2014**, *39*, 3516–3519. [CrossRef] [PubMed]
14. Wu, C.-Y.; Zou, Y.-H.; Timofeev, I.; Lin, Y.-T.; Zyryanov, V.Y.; Hsu, J.-S.; Lee, W. Tunable bi-functional photonic device based on one-dimensional photonic crystal infiltrated with a bistable liquid-crystal layer. *Opt. Express* **2011**, *19*, 7349–7355. [CrossRef] [PubMed]
15. Wang, H.-T.; Wu, P.-C.; Timofeev, I.V.; Zyryanov, V.Y.; Lee, W. Dynamic tuning and memory switching of defect modes in a hybrid photonic structure. *Crystals* **2016**, *6*, 129. [CrossRef]

16. Chilaya, G. Cholesteric Liquid Crystals: Optics, Electro-optics, and Photo-optics. In *Chirality in Liquid Crystals*; Kitzerow, H., Bahr, C., Eds.; Springer: New York, NY, USA, 2001; pp. 159–185.
17. Hsiao, Y.-C.; Tang, C.-Y.; Lee, W. Fast-switching bistable cholesteric intensity modulator. *Opt. Express* **2011**, *19*, 9744–9749. [CrossRef] [PubMed]
18. Patel, J.S.; Meyer, R.B. Flexoelectric electro-optics of a cholesteric liquid crystal. *Phys. Rev. Lett.* **1987**, *58*, 1538–1540. [CrossRef] [PubMed]
19. Wang, C.-T.; Wang, W.-Y.; Lin, T.-H. A stable and switchable uniform lying helix structure in cholesteric liquid crystals. *Appl. Phys. Lett.* **2011**, *99*, 041108. [CrossRef]
20. Wang, C.-T.; Lin, T.-H. Vertically integrated transflective liquid crystal display using multi-stable cholesteric liquid crystal film. *J. Disp. Technol.* **2012**, *8*, 613–616. [CrossRef]
21. Joo, S.-H.; Kim, J.-K.; Kim, H.; Shin, K.-C.; Kim, H.; Song, J.-K. Tri-stable polarization switching of fluorescent light using photo-luminescent cholesteric liquid crystals. *Mol. Cryst. Liq. Cryst.* **2014**, *601*, 29–35. [CrossRef]
22. Liu, Y.-J.; Wu, P.-C.; Lee, W. Spectral variations in selective reflection in cholesteric liquid crystals containing opposite-handed chiral dopants. *Mol. Cryst. Liq. Cryst.* **2014**, *596*, 37–44. [CrossRef]
23. Wu, P.-C.; Lisetski, L.N.; Lee, W. Suppressed ionic effect and low-frequency texture transitions in a cholesteric liquid crystal doped with graphene nanoplatelets. *Opt. Express* **2015**, *23*, 11195–11204. [CrossRef] [PubMed]
24. Kim, S.H.; Chien, L.-C.; Komitov, L. Short pitch cholesteric electro-optical device stabilized by nonuniform polymer network. *Appl. Phys. Lett.* **2011**, *96*, 161118. [CrossRef]
25. Nian, Y.-L.; Wu, P.-C.; Lee, W. Optimized frequency regime for the electrohydrodynamic induction of a uniformly lying helix structure. *Photonics Res.* **2016**, *4*, 227–232. [CrossRef]
26. Qutram, B.I.; Elston, S.J. Frequency-dependent dielectric contribution of flexoelectricity allowing control of state switching in helicoidal liquid crystals. *Phys. Rev. E* **2013**, *88*, 012506.
27. Lu, H.; Xu, W.; Song, Z.; Zhang, S.; Qiu, L.; Wang, X.; Zhang, G.; Hu, J.; Lv, G. Electrically switchable multi-stable cholesteric liquid crystal based on chiral ionic liquid. *Opt. Lett.* **2014**, *39*, 6795–6798. [CrossRef] [PubMed]

© 2017 by the authors. Licensee MDPI, Basel, Switzerland. This article is an open access article distributed under the terms and conditions of the Creative Commons Attribution (CC BY) license (http://creativecommons.org/licenses/by/4.0/).